Atmos. Chem. Phys., 8, 6261–6272, 2008
www.atmos-chem-phys.net/8/6261/2008/


Atmospheric Chemistry and Physics

# Absolute rate constant and O($^3$P) yield for the O($^1$D)+$N_2O$ reaction in the temperature range 227 K to 719 K

**S. Vranckx, J. Peeters, and S. A. Carl**

University of Leuven, Department of Chemistry, 200F Celestijnenlaan, 3001 Leuven, Belgium

Received: 4 March 2008 – Published in Atmos. Chem. Phys. Discuss.: 19 May 2008
Revised: 29 August 2008 – Accepted: 4 September 2008 – Published: 28 October 2008

**Abstract.** The absolute rate constant for the reaction that is the major source of stratospheric $NO_x$, O($^1$D)+$N_2O$ → products, has been determined in the temperature range 227 K to 719 K, and, in the temperature range 248 K to 600 K, the fraction of the reaction that yields O($^3$P). Both the rate constants and product yields were determined using a recently-developed chemiluminescence technique for monitoring O($^1$D) that allows for higher precision determinations for both rate constants, and, particularly, O($^3$P) yields, than do other methods. We found the rate constant, $k_{R1}$, to be essentially independent of temperature between 400 K and 227 K, having a value of $(1.37\pm0.11)\times10^{-10}$ cm$^3$ s$^{-1}$, and for temperatures greater than 450 K a marked decrease in rate constant was observed, with a rate constant of only $(0.94\pm0.11)\times10^{-10}$ cm$^3$ s$^{-1}$ at 719 K. The rate constants determined over the 227 K–400 K range show very low scatter and are significantly greater, by 20% at room temperature and 15% at 227 K, than the current recommended values. The fraction of O($^3$P) produced in this reaction was determined to be 0.002±0.002 at 250 K rising steadily to 0.010±0.004 at 600 K, thus the channel producing O($^3$P) can be entirely neglected in atmospheric kinetic modeling calculations. A further result of this study is an expression of the relative quantum yields as a function of temperature for the chemiluminescence reactions ($k_{CL1}$)$C_2H$ + O($^1$D) → CH(A) + CO and ($k_{CL2}$)$C_2H$ + O($^3$P) → CH(A) + CO, both followed by CH(A) → CH(X) + $h\nu$, as $k_{CL1}(T)/k_{CL2}(T)$=(32.8$T$−3050)/(6.29$T$+398).

*Correspondence to:* S. A. Carl
(shaun.carl@chem.kuleuven.be)

## 1 Introduction

The two most important reactions of electronically-excited atomic oxygen, O($^1$D), in the Earth's atmosphere are that with $H_2O$, which is the major source of OH radicals throughout the troposphere, and that with $N_2O$ in the stratosphere, producing directly NO and indirectly $NO_2$ via NO+$O_3$→$NO_2$+$O_2$. This latter reaction is part of the well-known chain mechanism that is crucial for determining stratospheric ozone concentrations (Crutzen et al., 1971), and of the $HO_x$, $ClO_x$, and $NO_x$ chain catalytic ozone destruction routes it has been demonstrated by Crutzen and Bruhl (2001) that the $NO_x$ sequence is the main cause of the spring to autumn stratospheric ozone decline in the Northern Hemisphere.

Besides in the atmosphere, reactions of O($^1$D) have also received attention due to their occurrence in gas-phase plasmas used in the oxidation of silicon surfaces (Kaspar et al., 2003) and in photochemical processes in other planetary atmospheres and around comets (Bhardwaj and Haider, 2002; Nair et al., 2005).

In this work we focus on the reaction of O($^1$D) with $N_2O$, which has seven exothermic product channels

| | | $\Delta_r H$(298 K) | |
|---|---|---|---|
| O($^1$D) + $N_2O$ | → $NO_2$ + N | −15 | (R1a) |
| | → $N_2$ + O($^3$P) + O($^3$P) | −23 | (R1b) |
| | → O($^3$P) + $N_2O$ | −190 | (R1c) |
| | → NO + NO | −341 | (R1d) |
| | → $O_2$($b^1\Sigma_g^+$) + $N_2$ | −364 | (R1e) |
| | → $O_2$($a^1\Delta_g$) + $N_2$ | −427 | (R1f) |
| | → $O_2$($X^3\Sigma_g^-$) + $N_2$ | −521 | (R1g) |

for which both direct and indirect quantification of the products, $N_2$, NO, and O($^3$P) have been employed to determine

product branching fractions. For the important NO channel, $k_{R1d}/k_{R1}$ appears to be reasonably well established at room temperature; a value of 0.61±0.06 (95% confidence) was recommended by Cantrell et al. (1994) following their own study and analysis of several studies by others up to 1994. The current recommended value of the JPL/NASA panel for stratospheric reactions (Sander et al., 2006) is in line with this at $k_{R1d}/k_{R1}$=0.6. To the authors' knowledge no direct experimental evidence for channel (R1a) has been reported. All O($^3$P) formed in the title reaction is assumed to be produced by channel (R1c), which is relatively minor at room temperature. An early study by Wine and Ravishankara (1982) established an upper limit for $k_{R1c}/k_{R1} \leq 0.04$, and a more recent determination by Nishida et al. (2004) gave $k_{R1c}/k_{R1}$=0.04±0.02. The rest of the reaction flux (ca. 35% to 40%) passes through either of, or a combination of, the last three channels (R1e)–(R1g) yielding $O_2$+$N_2$. The electronic state in which $O_2$ is preferentially produced is not established.

As well as the branching ratios, the overall rate constant, $k_{R1}$, has been determined in several studies, using a variety of methods (Carl, 2005, and references therein) for following the time profile of O($^1$D). The current NASA/JPL panel recommendation (Sander et al., 2006) for $k_{R1}$(298 K) is $(1.17\pm0.40)\times10^{-10}$ cm$^3$ s$^{-1}$, with the uncertainty representing approximately 95% confidence. This value is based on early $k_{R1}$ determinations by Davidson et al. (1979), Amimoto et al. (1979), Wine and Ravishankara (1981), and the very recent studies of Blitz et al. (2004), and Dunlea and Ravishankara (2004). Since the reported $k_{R1}$ values of the latter two studies differ by some 18% at room temperature and by almost 30% at lower stratospheric temperatures, no large improvement in the uncertainty of the recommended value over the previous recommendation was forthcoming. In fact the latest four determinations of $k_{R1}$ show a fair spread in values at room temperature. For the two studies mentioned above, Dunlea and Ravishankara (2004) determined $k_{R1}$ to be $(1.21\pm0.04)\times10^{-10}$ cm$^3$ s$^{-1}$, and Blitz et al. (2004) determined a value of $(1.07\pm0.08)\times10^{-10}$ cm$^3$ s$^{-1}$, whereas the latest two room-temperature determinations by Takahashi et al. (2005) and by Carl (2005) reported values of $(1.35\pm0.08)\times10^{-10}$ and $(1.43\pm0.08)\times10^{-10}$ cm$^3$ s$^{-1}$, respectively, where all values are given with their reported 95% confidence limits. During the preparation of this manuscript a room temperature determination for $k_{R1}$ of $(1.47\pm0.2)\times10^{-10}$ cm$^3$ s$^{-1}$ was reported by Dillon et al. (2008) as part of their study on the atmospheric chemistry of $SO_2F_2$.

The most extensive set of measurements to date are those above by Dunlea and Ravishankara (2004) for which twenty four determinations of $k_{R1}$ were carried out over the temperature range 220 K–370 K. Actually, the high stated precision of those determinations reveals a statistically significant difference between the weighted average of all nine 295 K data, $(1.21\pm0.04)\times10^{-10}$ cm$^3$ s$^{-1}$, and the $k_{R1}$(295 K) value of $(1.34\pm0.04)\times10^{-10}$ cm$^3$ s$^{-1}$ predicted from an Arrhenius fit to all other $k_{R1}(T)$ determinations of that study (fifteen in all). This, together with the most recent data of Takahashi et al. (2005) and Carl (2005), suggests that $k_{R1}$ is significantly greater than the current NASA/JPL recommendation, though still within its broad uncertainty limits.

The aim of the present study is three-fold. Firstly, to further reduce the uncertainty in $k_{R1}$ for this very important reaction by employing a recently-developed, highly-precise method (Carl, 2005) for the determination of O($^1$D) rate constants; secondly, to clearly establish its temperature dependence by extending $k_{R1}$ determinations to higher temperatures; and thirdly, to determine the branching fraction $k_{R1c}/k_{R1}$ over a wide temperature range to establish its value at stratospheric temperatures. High-temperature rate constant determinations could also aid predictions of stratospheric NO formation rates under conditions where the population of photolytically-produced O($^1$D) is not entirely thermalized before reaction with $N_2O$ (Kharchenko and Dalgarno, 2004).

## 2 Experimental section

We use a method to monitor O($^1$D), described recently by Carl (2005), based on the 431 nm CH(A→X) chemiluminescence resulting from the reaction,

$$C_2H + O(^1D) \rightarrow CH(A^2\Delta) + CO \qquad (R2)$$

Pulsed laser (10 ns) photolysis of the precursors $C_2H_2$ and $N_2O$, at 193 nm, generates the reactants of the above chemiluminescence reaction. Aside from production of O($^1$D), $N_2O$ photolysis at 193 nm results in a small fraction of O($^3$P) ($\Phi$(O($^1$D))=0.995, $\Phi$(O($^3$P))=0.005)) (Nishida et al., 2004). Additional O($^3$P) can result from O($^1$D) quenching by the precursor molecules $C_2H_2$ and $N_2O$, and by the bath gas He. The presence of O($^3$P) in the reaction volume also leads to CH(A→X) chemiluminescence by the analogous, but less efficient, reaction:

$$C_2H + O(^3P) \rightarrow CH(A^2\Delta) + CO \qquad (R3)$$

Rather than being a hindrance to the study of O($^1$D) reactions, the occurrence of reaction (R3) yields precise information on the fraction of O($^1$D) quenched during its reactive lifetime.

The radiative lifetime of CH(A) due to spontaneous emission is sufficiently short at ca. 540 ns (Luque and Crosley, 1996; Tamura et al., 1998) to ensure its concentration establishes a quasi-steady-state within a small time fraction of the O($^1$D) (or $C_2H$) decay time, such that the temporal profile of the 431 nm emission is determined by the temporal profiles of [O($^1$D)], [$C_2H$] and [O($^3$P)]. Both [O($^1$D)] and [$C_2H$] decay exponentially in the presence of excess reactants, while [O($^3$P)] resulting from O($^1$D) will be essentially determined

by the quenching kinetics owing to the negligible reactivity of O($^3$P) toward the molecular species present – in sharp contrast to O($^1$D) and $C_2H$. Thus, the widely differing reactivities of O($^1$D) and O($^3$P) result in a chemiluminescence profile that can be, for the sake of demonstration, easily separated into two components: the first arising from reaction (R2) and the second from reaction (R3).

The chemiluminescence intensity, $I_{\mathrm{chem2}}(t)$, due to Reaction (R2) is given by

$$I_{\mathrm{chem2}}(t) \propto k_{\mathrm{R2}}[\mathrm{O}(^1\mathrm{D})]_t[\mathrm{C_2H}]_t \quad (1a)$$

$$\propto k_{\mathrm{R2}}[\mathrm{O}(^1\mathrm{D})]_0[\mathrm{C_2H}]_0 \exp[-(k'_{\mathrm{O}(^1\mathrm{D})} + k'_{\mathrm{C_2H}})t] \quad (1b)$$

here $k'_{\mathrm{O}(^1\mathrm{D})}$ and $k'_{\mathrm{C_2H}}$ represent the total first-order decay rates of [O($^1$D)] and [$C_2H$], respectively, and [X]$_0$ refers to the concentration of X at $t$=0.

Given the negligible removal of O($^3$P) on the time scale of interest, its temporal concentration obeys the simple law $[\mathrm{O}(^3\mathrm{P})] \propto f_q[\mathrm{O}(^1\mathrm{D})]_{t=0}[1-\exp(-k'_{\mathrm{O}(^1\mathrm{D})}t)]$, where $f_q$ is the fraction of O($^1$D) that is quenched to O($^3$P), such that the chemiluminescence intensity due to Reaction (R3), $I_{\mathrm{chem3}}(t)$ is given by

$$I_{\mathrm{chem3}}(t) \propto k_{\mathrm{R3}}[\mathrm{O}(^3\mathrm{P})]_t[\mathrm{C_2H}]_t \quad (2a)$$

$$\propto k_{\mathrm{R3}} f_q[\mathrm{O}(^1\mathrm{D})]_0[1-\exp(-k'_{\mathrm{O}(^1\mathrm{D})}t)][\mathrm{C_2H}]_0 \exp(-k'_{\mathrm{C_2H}}t) \quad (2b)$$

For larger reaction times, $t > 5/k'_{\mathrm{O}(^1\mathrm{D})}$, [O($^3$P)] tends to $f_q$ [O($^1$D)]$_0$ , independent of time, and $I_{\mathrm{chem3}}(t) \propto k_{\mathrm{R3}} f_q$ [O($^1$D)]$_0$ [$C_2H$]$_0 \exp(-k'_{\mathrm{C_2H}}t)$. Thus, the values of both $k'_{\mathrm{O}(^1\mathrm{D})}$ and $k'_{\mathrm{C_2H}}$ could be determined by fitting the decay rates of $I_{\mathrm{chem}}(t) \equiv I_{\mathrm{chem2}}(t) + I_{\mathrm{chem3}}(t)$ at short times and at long times, respectively. This analysis is valid provided initial O($^3$P) formation is minor, such that the decay profile at short times is representative of O($^1$D) and $C_2H$ decay only. The full $I_{\mathrm{chem}}$ expression is given below in Eq. (4).

The ratio of the chemiluminescence channel rate coefficients $k_{\mathrm{R2}}$ and $k_{\mathrm{R3}}$ in Eqs. (1a, b) and (2a, b) is equal to 3.0±0.2 at room temperature. This ($T$-dependent) value was determined in this study by simply taking two chemiluminescence intensity profiles: one when photolysing a mixture of $N_2O$ and $C_2H_2$ in helium buffer gas, for which O($^1$D→$^3$P) quenching is negligibly slow, and the second when photolysing the same mixture in the presence of Ar or $N_2$, for which O($^1$D) is rapidly entirely quenched to O($^3$P). Indeed, the very low rate constant for O($^1$D) quenching by He, $<1\times10^{-15}$ cm$^3$ s$^{-1}$ (Dunlea and Ravishankara, 2004; Heidner et al., 1972) leads to a quenching rate of less than 300 s$^{-1}$ at 10 Torr He at room temperature (1 Torr=133 Nm$^{-2}$), which is negligible compared to the overall experimental O($^1$D) decay rates in the range 50 000 to 450 000 s$^{-1}$. On the other hand, both nitrogen and argon quench O($^1$D) rapidly, with rate coefficients of $(3.1\pm0.3)\times10^{-11}$ cm$^3$ s$^{-1}$ and $(8\pm3)\times10^{-13}$ cm$^3$ s$^{-1}$ at room temperature (Blitz et al., 2004), resulting in quenching rates at 10 Torr of $1.0\times10^7$ s$^{-1}$ and $2.6\times10^5$ s$^{-1}$ respectively. Thus, extrapolation of the emission intensities to $t$=0 and taking the ratio in $N_2$ (or Ar) over that in He gives $k_{\mathrm{R2}}/k_{\mathrm{R3}}$, provided that CH(A) is not significantly quenched by the buffer gas (Tamura et al., 1998).

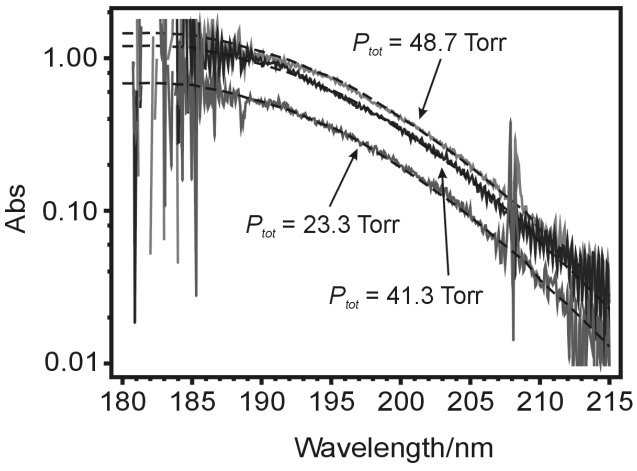


**Fig. 1.** Spectra of mixtures of 5% $N_2O$ in He taken in a single-pass absorption cell of 1.2 m length at three different total pressures. The fit to the data is based on the total cell pressure, the room temperature absorption cross-section of $N_2O$ and the fractional concentration of $N_2O$, which is the variable in the fit.

The concentration of each gas in the reaction chamber was calculated from the measured gas flows using the gas law together with the known fractional composition in the high-pressure cylinders. Though not a critical parameter we used the value of the fractional composition for $C_2H_2$ in He as that stated by the manufacturers of 0.0096. High-purity (99.9997%) helium was used as the bath gas for all kinetic experiments.

The concentration of $N_2O$ is, of course, an important parameter. The suppliers specification is 5.0% $N_2O$ in high-purity He. However, the fractional concentration of the cylinder was checked by single-pass uv optical absorption in a 1.2 m absorption cell using a $D_2$ lamp as the light source. The resulting spectra together with fits using the known absorption cross sections (Sander et al., 2006; Selwyn et al., 1977) are displayed in Fig. 1. Our fits give the percentage of $N_2O$ in the cylinder as (5.10±0.30)% (95% confidence).

The possible impurities of the $N_2O$/He cylinder were also checked by electron-impact ionization mass-spectrometry, in which several mass spectra were taken as a function of electron energy to eliminate ions resulting from $N_2O$ fragmentation from the analysis. Here only trace amounts of NO and $N_2$ were detected and their estimated mole fractions of less than $1\times10^{-6}$ were too small to significantly influence the kinetic measurements.

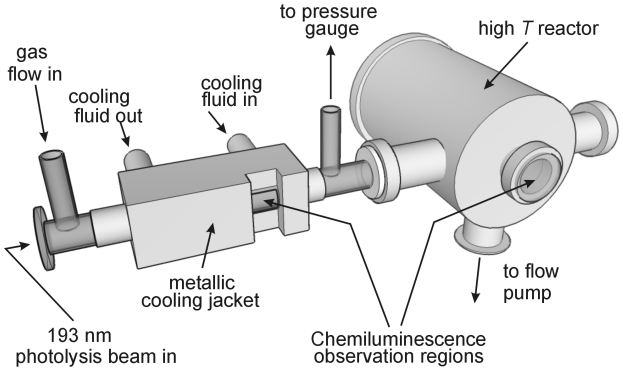


**Fig. 2.** Experimental apparatus showing the coupled low- and high-temperature reaction cells used for the determination of $k_{R1}(T)$ and for the O($^3$P) yield $k_{R1c}/k_{R1}$.

Typical 193 nm laser intensity for these experiments was 15 mJ cm$^{-2}$. This intensity results in a fraction of $C_2H_2$ dissociated as 0.0026 and a fraction of $N_2O$ dissociated as 0.0014. On average ca. $1\times10^{12}$ O($^1$D) cm$^{-3}$ and ca. $4\times10^{11}$ $C_2H$ cm$^{-3}$ are produced per laser pulse.

The experimental setup is illustrated in Fig. 2. To enable a large range of temperatures to be covered, two reaction vessels of entirely different construction were connected in series, such that the photolysis laser beam was able to pass through both of them at the same time.

The reactor on the left in Fig. 2 is made of a single tube of chemically-inert PFA (perfluoroalkoxy) of internal diameter 10 mm and length 30 cm with a gas inlet and outlet. As connections to the single Spectrosil quartz window of the PFA reactor and for the gas inlet and pressure meter, PFA Swagelock "Tee" connectors were used (not shown). This reactor was designed to cover the ranges from ca. 500 K to ca. 220 K. It is cooled or heated by fluid flowing in a closed circuit through a metallic jacket surrounding the PFA reactor tube. There is a quartz entrance window for the laser beam; the exit window is placed after passage through the second reactor volume. Interestingly, no window for detection of the chemiluminescence is required for the PFA reactor: the PFA tubing is partially transparent to the 431 nm chemiluminescence and according to our test does not significantly fluoresce at this wavelength on passage of the uv photolysis pulse. The chemiluminescence detection system comprises a lens, an interference filter (430±10 nm) and a photomultiplier tube that are placed close to the PFA reactor, and arranged such that the chemiluminescence is detected at right-angles to the passage of the laser beam. For this, the metallic cooling jacket exposes the PFA tube on one side for 3 cm at about 3/4 along its length. The cooling fluid was maintained at the correct temperature by a commercial temperature controller. Pressure in the reaction cell was determined using a calibrated capacitance manometer that was cross-checked regularly with other calibrated pressure gauges. The pressure measurement point was located about 12 cm downstream of the chemiluminescence observation zone, using a second PFA Swagelock "Tee" connector (not shown) placed between the two reactors. At the flow rates used in this experiment there was negligible pressure drop between the observation point and the pressure-measurement point. Upstream of the reactor, the separate flows of He, $C_2H_2$/He, and $N_2O$/He, were combined in a small volume to ensure complete mixing before entering the reactor.

The reactor on the right is a larger heatable stainless steel cell that has been used for many previous studies for $C_2H$, OH, and $CF_2$ reactions (Elsamra et al., 2005; Khamaganov et al., 2006; Dils et al., 2004). It can cover a temperature range of 290 K to 850 K. A glass window is used as exit window for the chemiluminescence, detected perpendicular to the axis of the laser beam. The interference filter, collection lens and PMT are mounted together on a translation stage such that they are easily moved between the observation points of the two reaction cells, thus providing a very convenient way to directly compare rate constants at two different temperatures if need be.

The temperature of the gas mixture in the reaction cells was measured using retractable calibrated thermocouples. We estimate the uncertainties in temperature to be ±10 K at 719 K decreasing to ±1 K at room temperature and then to increase again to 220 K to ±5 K, all at ca. 95% confidence.

## 3 Results and discussion

### 3.1 Determination of $k_{R1}(T)$

Preliminary results revealed a very small O($^3$P) yield for the title reaction, in qualitative agreement with the previous studies mentioned above. Thus, under the conditions used for the rate constant determinations, the chemiluminescence decay profiles are effectively single exponential at short times ($t\leq10\ \mu$s) and represent the sum of the decay rates of O($^1$D) and $C_2H$ only, with interference from any growth of O($^3$P) therefore negligible. In fact, even for reactions with substantial quenching to O($^3$P) the decay rate of O($^1$D) alone is in principle relatively easily extracted as described previously (Carl, 2005). Here though, the determination of $k_{R1}$ is more transparent as it involves fitting to a single-exponential decay only.

A typical chemiluminescence time profile generated using our new method is displayed in the log-linear plot of Fig. 3. The tail observed at long times results from O($^3$P) formation (see above), but does not affect the extraction of the O$^1$D decay rate.

Here the total decay constant, neglecting the slow quenching of O($^1$D) by He, is given by

$$k'_{tot} = k'_{O(^1D)} + k'_{C_2H} = \quad (3)$$
$$\left(k_{C_2H+C_2H_2}+k_{O(^1D)+C_2H_2}\right)[C_2H_2] + \left(k_{C_2H+N_2O}+k_{R1}\right)[N_2O]$$

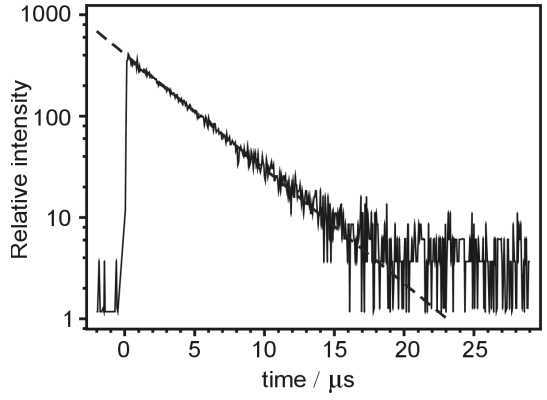


**Fig. 3.** A typical chemiluminescence decay profile observed following 193 nm photolysis of $C_2H_2/N_2O$/He mixtures at 10 Torr total pressure. The decay rate represents the sum of decay rates of $C_2H$ and O($^1$D). The small "tail" visible after ca. 17 $\mu$s is indicative of O($^3$P) formation from channel (R1c) or directly from $N_2O$ photolysis. The exponential fit was performed over the range 1 $\mu$s to 20 $\mu$s in this case.

The solid line is a single-exponential fit to the data, neglecting the longer-time portion that includes chemiluminescence arising from a small fraction of O($^3$P) produced by quenching of O($^1$D).

Our recent detailed experimental and theoretical investigation of the $C_2H+N_2O$ reaction (manuscript in preparation) shows it to have a significant barrier and a low rate constant ranging from (an extrapolated) $\approx 10^{-16}$ cm$^3$ s$^{-1}$ at 300 K to ca. $1\times10^{-13}$ cm$^3$ s$^{-1}$ at 750 K. Thus, over the 300–750 K range, for the present experimental [$N_2O$] of $1\times10^{14}$ cm$^{-3}$ to $2.5\times10^{15}$ cm$^{-3}$ the removal rate of $C_2H$ by $N_2O$ is less than 0.1% of the removal rate of O($^1$D) by $N_2O$. Therefore, plots of $k'_{tot}$ versus [$N_2O$] at constant [$C_2H_2$] should yield a gradient equal to $k_{R1}$. Figure 4 shows examples of such $k_{R1}$ determinations at 227 K, 298 K and 422 K. The ordinate intercepts correspond to the sums of the known removal rates of O($^1$D) and $C_2H$ by $C_2H_2$, with rate constants at 295 K of $3.08\times10^{-10}$ cm$^3$ s$^{-1}$ and $1.3\times10^{-10}$ cm$^3$ s$^{-1}$, respectively (Carl, 2005; Van Look and Peeters, 1995; Vakhtin, 2001). That, our $k_{C_2H+N_2O}$ was found to be very small at room temperature provides additional support of the high purity of the $N_2O$ mixture used for the O($^1$D) experiments, given the general high reactivity of $C_2H$, especially toward hydrocarbons.

The high precision of the data in the plots of Fig. 4 is typical of our chemiluminescence method, which allows O($^1$D) removal rates of up to 450 000 s$^{-1}$ to be measured. Note that the data presented in this study, including those taken at room temperature, were determined on four separate occasions over a period of several months and using two different reactors and different sets of calibrated flow controllers. Back-to-back runs of rate constant determinations confirmed this high precision, with only ±3% variation in rate constants from the mean.

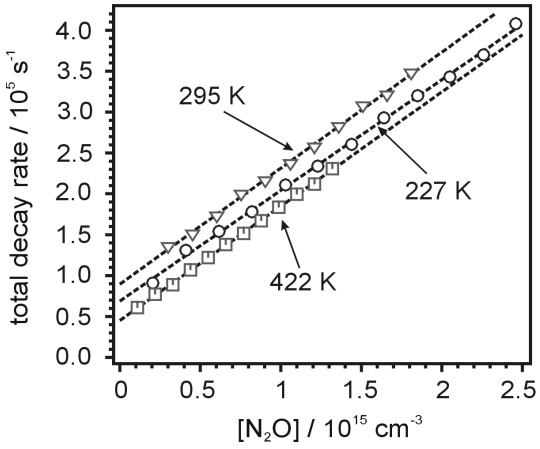


**Fig. 4.** The total decay rates as a function of $N_2O$ concentration. Conditions for 227 K: [$C_2H_2$]≅$1.0\times10^{14}$ cm$^{-3}$, $N_2O$ concentrations range from $2.05\times10^{14}$ to $2.46\times10^{15}$ cm$^{-3}$, result: $k_{R1}=(1.35\pm0.03)\times10^{-10}$ cm$^3$ s$^{-1}$. Conditions for 295 K: [$C_2H_2$]=$1.5\times10^{14}$ cm$^{-3}$, total pressure 10 Torr He and [$N_2O$] ranges from $3.0\times10^{14}$ cm$^{-3}$ to $1.82\times10^{15}$ cm$^{-3}$, result: $k_1=(1.40\pm0.04)\times10^{-10}$ cm$^3$ s$^{-1}$. Conditions for 422 K: [$C_2H_2$]=$5.5\times10^{13}$ cm$^{-3}$, total pressure 10 Torr He and [$N_2O$] ranges from $1.10\times10^{14}$ cm$^{-3}$ to $1.32\times10^{15}$ cm$^{-3}$, result: $k_1=(1.40\pm0.02)\times10^{-10}$ cm$^3$ s$^{-1}$.

The results of all $k_{R1}$ rate constant determinations are given in Fig. 5, together with the results of the most recent studies by other groups (Blitz et al., 2004; Dunlea and Ravishankara, 2004; Takahashi 2005). The $k_{R1}$ values are also listed in Table 1 along with three columns of uncertainties. The first of these gives the 95% confidence limits in the fitted slopes for plots such as those given in Fig. 4 that are derived statistically from the weighted least-squares fitting procedure. For fitting a suitable function to the data, the relative weights of the individual data points need to be estimated. The random uncertainties on individual determinations just mentioned (column 3 of Table 1) should not, in this case, be used as relative weighting factors, as this would imply, for example, that the confidence in the value at 227 K is a factor four greater than that at 447 K, whereas it is noted that the scatter of the data is greater than the random uncertainty associated with many of the individual determinations, including the one at 227 K. In fact the scatter of the data around some mean value – given by the standard deviation – has two random error contributions. One of these is a pooled average of the individual uncertainties; the other represents the random error introduced by repeating an experiment, which is likely due mainly to uncertainties in flow controller calibrations. To determine the average scatter of the data points we consider the data in the range 227 K to 447 K and assume $k(T)$ it to be constant (this will tend to overestimate the scatter). Thus, the standard deviation, SD, is $0.045\times10^{-10}$ cm$^3$ s$^{-1}$. An estimate of the likely spread in the data at 95% confidence is

**Table 1.** Summary of rate constant determinations for O($^1$D) + $N_2O$ of this work.

| $T$/K | $k_{R1}/10^{-10}$ cm$^3$ s$^{-1}$ | Uncertainty in the gradient ($10^{-10}$ cm$^3$ s$^{-1}$)[a] | Estimated statistical uncertainty in $k_{R1}/10^{-10}$ cm$^3$ s$^{-1}$[a] | $\Delta k_{R1}/10^{-10}$ cm$^3$ s$^{-1}$[a] |
|---|---|---|---|---|
| 227 | 1.35 | ±0.03 | ±0.09 | ±0.12 |
| 234 | 1.33 | ±0.02 | ±0.09 | ±0.12 |
| 235 | 1.35 | ±0.03 | ±0.09 | ±0.12 |
| 245 | 1.36 | ±0.04 | ±0.09 | ±0.12 |
| 250 | 1.34 | ±0.03 | ±0.09 | ±0.12 |
| 256 | 1.41 | ±0.04 | ±0.09 | ±0.13 |
| 258 | 1.30 | ±0.04 | ±0.09 | ±0.12 |
| 261 | 1.40 | ±0.03 | ±0.09 | ±0.12 |
| 293 | 1.35 | ±0.03 | | |
| 295 | 1.32 | ±0.09 | | |
| 295 | 1.38 | ±0.10 | | |
| 295 | 1.28 | ±0.02 | | |
| 295 | 1.40 | ±0.04 | ±0.016 | ±0.08 |
| 295 | 1.43 | ±0.04 | | |
| 295 | 1.41 | ±0.02 | | |
| 295 | 1.35 | ±0.04 | | |
| 295 | 1.41 | ±0.02 | | |
| 351 | 1.36 | ±0.03 | ±0.09 | ±0.12 |
| 392 | 1.44 | ±0.03 | ±0.09 | ±0.12 |
| 422 | 1.40 | ±0.02 | ±0.09 | ±0.12 |
| 446 | 1.30 | ±0.12 | ±0.15 | ±0.17 |
| 552 | 1.19 | ±0.02 | ±0.09 | ±0.11 |
| 614 | 1.24 | ±0.19 | ±0.21 | ±0.22 |
| 638 | 1.11 | ±0.05 | ±0.10 | ±0.12 |
| 719 | 0.94 | ±0.05 | ±0.10 | ±0.11 |

[a] Column 3 gives the uncertainties at 95% confidence in the slope of the corresponding plot of O($^1$D) removal rate versus [$N_2O$] concentration. Column 4 gives the expected total random error of $k$ at each temperature. Column 5 gives the estimated total uncertainty in $k$, which includes the systematic uncertainty on the $N_2O$ concentration (identical for all data). The values in italics in columns 3 and 4 for the room-temperature data are the 95% confidence limits in the mean value.

$\pm 2\times$SD=$\pm 0.090\times10^{-10}$ cm$^3$ s$^{-1}$. The average contribution to this value of the uncertainties of individual determinations is $(N/\Sigma_i(1/s_i^2))^{0.5}$=$0.029\times10^{-10}$ cm$^3$ s$^1$, where $s_i$ are the 95% confidence on individual determinations and $N$ is the number of data points considered. Thus the contribution, at 95% confidence, of experiment repeatability to $2\times$SD is $(0.090^2–0.029^2)^{0.5}\times10^{-10}$ cm$^3$ s$^{-1}$=$0.085\times10^{-10}$ cm$^3$ s$^{-1}$. This last value is now propagated with the uncertainty of each data point (column 3 Table 1) to give an estimate of the relative weights of the data. These are given in column 4 of Table 1 and also plotted as error bars in Fig. 5. Using these values as error bars is somewhat artificial since they have been derived partly from the data itself, however they do give a visual representation of the relative weights of the data points. Additional to those random errors, is the systematic uncertainty of ca. 6% in the fractional concentration of $N_2O$ of our cylinder that was based on analysis of the results of our absorption measurements. This uncertainty, which applies equally to all points with the same sign, affects only the absolute value of the whole set of rate constant data and not their temperature dependence. It is statistically added to the overall errors at 95% confidence in the final column. These overall uncertainties cannot be used in a least-squares fitting procedure of the data. We estimate our confidence in temperature of the monitored reaction zone (at ca. 95% limits) to be ±10 K at 719 K, ±4 K at 446 K, decreasing to ±1 K at room temperature and then to increase again to 220 K to ±5 K. In the 446 K to 227 K temperature range consideration of the uncertainty in temperature leads to an additional uncertainty in [$N_2O$] and therefore in the determined rate constants. The greatest effect will be for the 227 K data point for which an additional uncertainty in $k_{R1}$ of $\pm0.03\times10^{-10}$ cm$^3$ s$^{-1}$. If these temperature uncertainties are considered to be random and uncorrelated then they can be propagated with the $0.085\times10^{-10}$ cm$^3$ s$^{-1}$ 95% confidence value given above. This leads to $(0.085^2+0.03^2)^{0.5}\times10^{-10}$ cm$^3$ s$^{-1}$ = $0.090\times10^{-10}$ cm$^3$ s$^{-1}$. There is however likely to be some correlation between

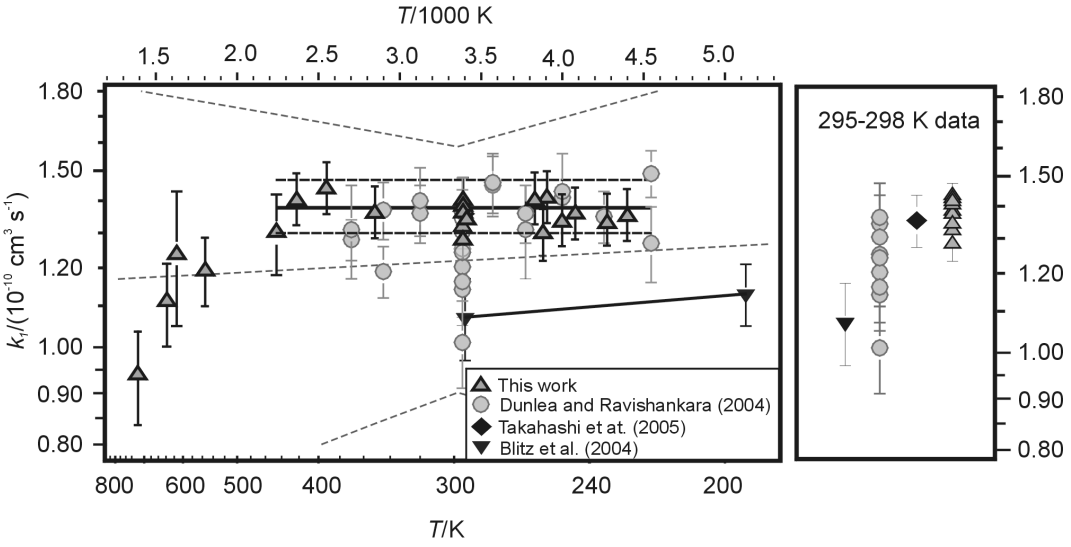


**Fig. 5.** Summary of the results obtained for $k_1$ plotted as a function of temperature together with the three most recent results of Blitz et al. (2004), Dunlea and Ravishankara (2004) and Takahashi et al. (2005). The dotted line through the middle of the graph and the outer dotted lines represent the current JPL/NASA recommendation and its ca. 95% uncertainty limits, respectively. The inner lines represent the best fit to our data between 227 K and 446 K assuming a $T$-independent $k_{R1}$ and 95% confidence limits that includes the 6% uncertainty in the $N_2O$ fraction. The plot on the right better shows individual room-temperature determinations of this work and those from the most recent studies by other groups.

the temperature uncertainties at various temperatures. In an extreme case all temperatures below room temperature would be overestimated by the 95% confidence values and all above room temperature would be underestimated by their 95% confidence values. A best straight line fit to corrected rate constants in this case passes through 1.39±0.03 at 220 K, through 1.37±0.01 at 300 K to 1.35±0.03, where the uncertainties indicate the extent of the 95% confidence bands.

All of our $k_{R1}$ values below 450 K are significantly greater than the current recommendation. Between 227 K and 446 K the determined values – twenty one in all – range from $1.28\times10^{-10}$ cm$^3$ s$^{-1}$ to $1.43\times10^{-10}$ cm$^3$ s$^{-1}$ (standard deviation of $0.05\times10^{-10}$ cm$^3$ s$^{-1}$) with a weighted mean of $(1.37\pm0.02)\times10^{-10}$ cm$^3$ s$^{-1}$ at 95% confidence (excluding the uncertainty in [$N_2O$]). That the rate constant shows a marked decrease beyond 450 K strongly suggests that, in the range 227 K to 446 K, it should either decrease slightly with increasing temperature or remain approximately constant. Since our data indicates a slight increase in $k_{R1}$ over this range and taking into account possible systematic, correlated errors in reactor temperature, we suggest a constant value of $(1.37\pm0.11)\times10^{-10}$ cm$^3$ s$^{-1}$ at 95%, which also includes the 6% uncertainty in our $N_2O$ fraction. These full confidence limits are plotted as dashed lines around the mean value in Fig. 5.

This value is in excellent agreement with the room temperature study of Takahashi et al. (2005) of $(1.35\pm0.06)\times10^{-10}$ cm$^3$ s$^{-1}$ as well as the average of all determinations (beside those at room temperature, as discussed in the Introduction) by Dunlea and Ravishankara (2004) of $(1.34\pm0.04)\times10^{-10}$ cm$^3$ s$^{-1}$. The results of recent determinations of rate constant for O($^1$D)+$N_2O$ by other groups is also given in tabular form (Table 2).

The rate constants determined in this work decrease markedly beyond about 450 K. This effect is not unusual if the so-called "bottle-neck structure" is located on a purely attractive entrance part of the potential energy surface (see Forst, 2003). Conservation of the rotational quantum number $J$ during the reaction means that the amount of energy available for random distribution amongst all other modes changes as the reactants approach one another. The bottle-neck structure is the structure (or point on the potential energy hypersurface) that has a minimum number of states, counted from the zero-point energy to total available randomizable energy for that structure. As the reactants approach and the overall moment of inertia decreases, the energy associated with $J$, $E_J$, increases leading to proportionally less energy available for randomization. The total available randomizable energy (and therefore the number of states) depends therefore both on the shape of the potential energy surface and on how $E_J$ changes over the surface. The first is independent of temperature whereas the latter is temperature dependent. At higher temperatures, the differences in $E_J$ over the surface become more pronounced with the result that the bottle-neck structure – which will also change with temperature – has proportionally fewer available randomizable states. This leads to a decrease in rate constant with increasing temperature.

**Table 2.** Summary of recent determinations of the rate constant determinations for O($^1$D) + $N_2O$ by others groups. The first three are plotted in Fig. 5.

| $T$/K | Dunlea and Ravishankara (2004) | Blitz et al. (2004) | Takahashi et al. (2005) | Amimoto et al. (1979) |
|---|---|---|---|---|
| 195 | | 1.13±0.08 | | |
| 220 | 1.27±0.11 | | | |
| 220 | 1.49±0.08 | | | |
| 235 | 1.35±0.08 | | | |
| 250 | 1.41±0.15 | | | |
| 250 | 1.43±0.13 | | | |
| 265 | 1.31±0.14 | | | |
| 265 | 1.36±0.09 | | | |
| 280 | 1.46±0.10 | | | |
| 280 | 1.45±0.10 | | | |
| 295 | 1.21±0.04[a] | 1.07±0.10[b] | 1.35±0.08 | 1.2±0.1 |
| 320 | 1.40±0.11 | | | |
| 320 | 1.36±0.09 | | | |
| 345 | 1.19±0.07 | | | |
| 345 | 1.37±0.09 | | | |
| 370 | 1.31±0.14 | | | |
| 370 | 1.28±0.06 | | | |

[a] Weighted average of fifteen determinations.
[b] Rate constant at 294 K.

A similar effect can be caused by partial re-dissociation of an initially-formed reaction complex. In this case there is an increased propensity to re-dissociate to reactants over the entrance-channel transition state rather than undergo transformation via a second transition state (that can lie lower in energy than the reactants) leading to products.

### 3.2 Determination of the O($^3$P) yield

For the accurate interpretation of O($^3$P) yields from Reaction (R1), sources of potential interferences need to be considered. The first of these is direct production of O($^3$P) from the 193 nm photo-dissociation of $N_2O$. The quantum yield for this process had been recently determined by Nishida et al. (2004) as $\Phi_{O(^3P)}$=0.005±0.002. Thus, from this process alone, our uncertainty in the determined O($^3$P) yield from Reaction (R1) would be ±0.002.

Note that $O_2$ or $N_2$ impurities, e.g. from air leaks, could affect the results by chemiluminescence via $C_2H+O_2 \rightarrow CH(A)+CO_2$ (Elsamra et al., 2005) or by O($^1$D→$^3$P) quenching. It was duly ascertained in this work that the $O_2$ and $N_2$ traces were so small as to have an entirely negligible effect. We must now conclude that the anomalously high quenching fraction value of 0.056 reported in the earlier investigation of this laboratory by Carl (2005) was most likely due to a very small air leak in the reactor, whose influence may have been amplified due to its proximity to the chemiluminescence observation zone.

The general equation for the chemiluminescence decay profile is (Carl, 2005)

$$I_{\text{chem}} = B\,[C_2H]_t \left[ \left[O(^1D)\right]_t + \frac{\left[O(^3P)\right]_t}{k_{R2}/k_{R3}} \right] \quad (4)$$

$$\left[O(^1D)\right]_t = \left[O(^1D)\right]_0 \exp(-k'_{O(^1D)}t) \quad (5)$$

$$k'_{O(^1D)} = k_{O(^1D)+C_2H_2}\,[C_2H_2] + k_{O(^1D)+N_2O}\,[N_2O] + k_{O(^1D)+N_2}\,[N_2] + k_{O(^1D)+He}\,[He] \quad (6)$$

$$[C_2H]_t = [C_2H]_0 \exp(-k'_{C_2H}t) \quad (7)$$

$$k'_{C_2H} = k_{C_2H+C_2H_2}\,[C_2H_2] + k_{C_2H+N_2O}\,[N_2O] \quad (8)$$

O($^3$P) production via O($^1$D) reaction with or quenching by $C_2H_2$, $N_2O$, $N_2$, and He, together with instantaneous O($^3$P) formation via $N_2O$ photolysis leads to the expression

$$\left[O(^3P)\right]_t = \left[O(^1D)\right]_0 \left(0.005 + \frac{k'_P}{k'_{O(^1D)}} \left[1 - \exp(-k'_{O(^1D)}t)\right]\right) \quad (9)$$

$$k'_p = k_{O(^1D)+C_2H_2}\,[C_2H_2]\,Q_{C_2H_2} + k_{O(^1D)+N_2O}\,[N_2O]\,Q_{N_2O} + k_{O(^1D)+N_2}\,[N_2] + k_{O(^1D)+He}\,[He] \quad (10)$$

with $Q_x$ the fractional yield of O($^3$P) from the reaction O($^1$D)+X; $Q_x$=1 for $X$=$N_2$, and He.

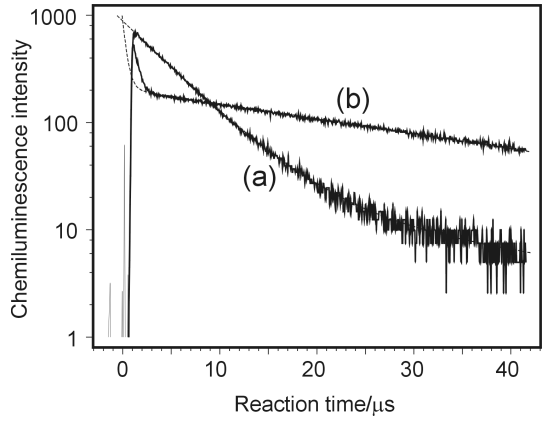


**Fig. 6.** An example of the change in chemiluminescence decay profile on addition of $N_2$ to the reactor. The chemiluminescence signal of profile **(a)** was taken following photo-dissociation of a small fraction of $N_2O$ and $C_2H_2$in He. The decay rate is proportional to the sum of decay rates of [$C_2$H] and [O($^1$D)] and the intensity is proportional to [$C_2$H][O($^1$D)]$k$($C_2$H+O($^1$D)→CH(A)+CO). Profile **(b)** was recorded under exactly the same conditions as for profile (a) except that a small fraction of the He flow was replaced by $N_2$ flow. In this case, O($^1$D) is rapidly quenched by $N_2$ O($^3$P). Here, except at short times, the decay rate is that of [$C_2$H] only and the intensity proportional to [$C_2$H][O($^3$P)]$k$($C_2$H+O($^3$P)→CH(A)+CO). The dotted lines are expected time profiles of the chemiluminescence signals in each case. For profile (b), at $0<t<2$ $\mu$s, a deviation from the expected profile is seen due to the time constant of the collection electronics. The ratio of the extrapolated intensities of the two exponential profiles to $t$=0 gives the ratio of the rate constants for the two chemiluminescence reactions considered in the paper.

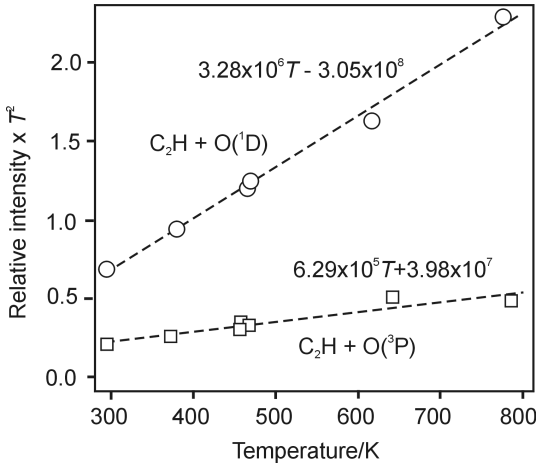


**Fig. 7.** The relative chemiluminescence intensity at $t$=0 (extrapolated from the total decay) multiplied by $T^2$. Conditions: [$N_2O$]=7.44×10$^{14}$ cm$^{-3}$×$T$/298, [$C_2H_2$]=1.49×10$^{14}$ cm$^{-3}$×$T$/298, total pressure 2 Torr He for $C_2$H+O($^1$D), 2 Torr $N_2$ for $C_2$H+O($^3$P), $T$ varies from 298 K to 797 K.

The ratio $k_{R2}(T)/k_{R3}(T)$, was experimentally determined using our new detection method for O($^1$D) and O($^3$P). An absolute determination of either $k_{R2}$ or $k_{R3}$ as a function of temperature was not possible here because the absorption cross-section of the oxygen atom precursor, $N_2O$, is not accurately known as a function of the temperature. However, it was possible to determine their ratio, as described in the experimental section. Thus, the ratio of initial chemiluminescence intensities, one taken with buffer gas He that does not contribute to any O($^1$D →$^3$P) quenching, and the other with buffer gas $N_2$ that rapidly quenches all initial O($^1$D) to O($^3$P), is given by

$$\frac{I_{\text{chem(He)t}\to 0}}{I_{\text{chem(N2)t}\to 0}} = \frac{k_{R2}}{k_{R3}} \tag{11}$$

neglecting the small fraction of O($^3$P) produced directly by $N_2O$ photolysis (Nishida et al., 2004).

Since all experiments to determine $k_{R2}(T)/k_{R3}(T)$ were performed with identical total- and partial flow rates, at the same pressure, and using the same photolysis energy, the concentrations of $C_2H_2$ and $N_2O$ scale each as $1/T$. Thus the chemiluminescence signal would scale as $1/T^2$ if $k_{R2}$ or $k_{R3}$ were independent of temperature. For increased accuracy, rather than the ratio $k_{R3}/k_{R2}$ being determined at each temperature, $k_{R3}(T)$ and $k_{R2}(T)$ were determined separately and then $k_{R3}/k_{R2}$ was accurately determined at 295 K. An example of temporal chemiluminescence profiles with He buffer gas and with $N_2$ buffer gas is given in Fig. 6. Profile (a) with He has a time dependence governed by both [$C_2$H] and [O($^1$D] and an intensity essentially proportional to $k_3$($C_2$H+O($^1$D)→CH(A)+CO) whereas profile (b) has a time profile governed by [$C_2$H] only and an intensity proportional to $k_{R2}$($C_2$H+O($^3$P)→CH(A)+CO) except at short times where O($^1$D) quenching occurs. Plots of $I_{\text{chem}}$(He or $N_2)_{t\to 0}\times T^2$ versus $T$, are given in Fig. 7. The ratio of the fitted $I_{\text{chem,t}\to 0}$ of each set of experiments gives then the ratio of the two rate coefficients as a function of temperature.

$$\frac{k_{R2}(T)}{k_{R3}(T)} = \frac{32.8T - 3050}{6.29T + 398} \tag{12}$$

In fact the temperature dependence given by the denominator, which is the sum of the $T$ dependence of $k_3$ and the $T$ dependence of $\sigma(N_2O)$ at 193 nm (assuming $\Phi$(O$^1$D)=1) is quite similar to that found by Devriendt et al. (1996) for the $T$ dependence of $k_3$ alone. This indicates that $\sigma(N_2O)$ changes by a factor 1.5 at most between 300 K and 800 K.

For the O($^3$P) yield determinations, a typical decay profile is given in Fig. 8. One can immediately see that the chemiluminescence signal due to O($^1$D) is at least a factor 100 greater than that of the due to O($^3$P). This immediately suggests an O($^3$P) yield of 0.03 at most, bearing in mind the that $k_{R3}/k_{R2}$=3.0 at room temperature and that reaction with $N_2O$ is the dominant O($^1$D) removal process. Also shown is the best fit to the data as well as three simulations. The flexible parameters in the fit equations are the total first-order removal rate of [O($^1$D)], $k'_{O1D}$, the total first-order removal

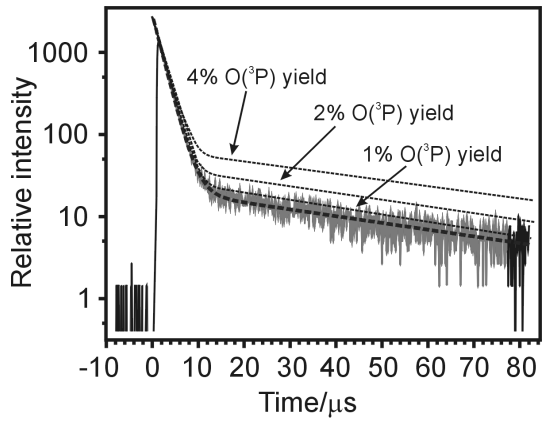


**Fig. 8.** O($^3$P) yield investigations. CH(A→X) emission profile for the following from CH(A) formed through $C_2H$+O($^1$D) and $C_2H$+O($^3$P). Conditions: $[N_2O]=3.21\times10^{15}$ cm$^{-3}$, $[C_2H_2]=6.96\times10^{13}$ cm$^{-3}$, total pressure 10 Torr He, 247 K. The bold dashed line is the best fit of the function of Eq. (7) to the decay. In this case the adjustable parameter $Q_{N_2O}(=k_{R1c}/k_{R1})=0.02\pm0.02$. Also plotted are simulated curves for $Q_{N_2O}$=0.01, 0.02, and 0.04. Note that $Q_{N_2O}$=0.04 was found by Nishida et al. (2004) and was suggested as an upper limit by Wine and Ravishankara (1982).

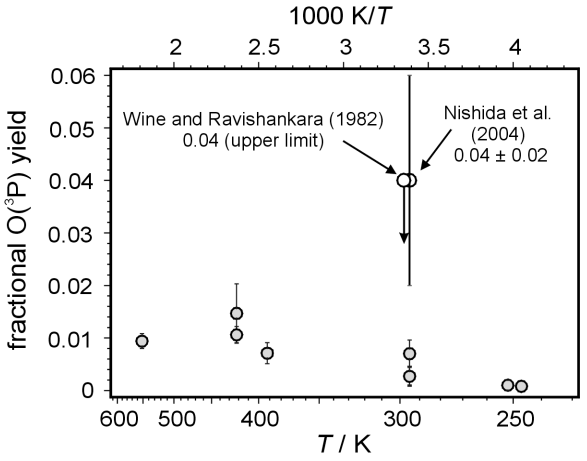


**Fig. 9.** Summary of the results of the determinations of $k_{R1c}/k_{R1}$. All error bars indicate 95% confidence.

rate for $C_2H$, $k'_{C_2H}$, the scaling factor $B$, and the fractional yield of O($^3$P) from Reaction (R1), $Q_{N_2O}$, i.e. the value to be determined. The other parameters are fixed to their measured values, all of which are given above.

Importantly, the removal rates $k'_{O^1D}$ of O($^1$D) and $k'_{C_2H}$ of $C_2H$ found through fitting the decays are to within a few percent equal to the values calculated from the experimental concentrations and known rate coefficients.[1] Note also, that under the conditions of these sets of experiments the O($^1$D) removal rate is determined almost uniquely by the title reaction, such that the determined O($^3$P) yield from the fit to the chemiluminescence decay profile is quasi-insensitive to the values of the other parameters.

The results of all determinations of the O($^3$P) yield from the title reaction, such as the one given in Fig. 8, are summarized in Fig. 9 together with the results of earlier studies of Wine and Ravishankara (1982) and Nishida et al. (2004).

The results clearly show the yield of O($^3$P) to be less than 0.01 over the temperature range 550 K to 250 K, slightly decreasing with decreasing temperature. At the lowest temperature of ca. 250 K an upper limit for the O($^3$P) yield of 0.002 could be established. These values rely partly of course on the single O($^3$P) quantum yield determination Nishida et al. (2004) in that we observe in this study the sum of both quenching to O($^3$P) and direct photolytic production. If one considers the O($^3$P) quantum yield for $N_2O$ photolysis at 193 nm is to be zero, then all of the above values for the O($^1$D) quenching fraction would be increased by approximately 0.005. In any case, channel (1c) need not be taken into consideration in stratospheric chemistry models.

The overall impact of the study related here has been firstly to provide a set of $k_{R1}(T)$ data that taken with that of Dunlea and Ravishakara (excepting their anomalously low 295 K data) and of Takahishi et al. (2005) – all performed using different methods for O($^1$D) detection – is to substantially reduce the uncertainty in the overall rate constant for this reaction, and to significantly increase its best estimate, to be used in atmospheric chemistry models. The impact of our recommended values on modeling calculations naturally depends on values currently adopted for a particular model. At one extreme, models that rely on the JPL/NASA recommendations prior to 2006 with an overall $T$-independent rate constant $k_{R1}=1.16\times10^{-10}$ cm$^3$ s$^{-1}$, that interpret the branching of 0.60 as $k_{R1d}/(k_{R1e}+k_{R1f}+k_{R1g})$, and not $k_{R1d}/k_{R1}$, and then consider an additional reduction of $k_{1d}$ by 4% due to channel (1c), as discussed by Nishida et al. (2004), effectively use a value for the NO channel $k_{R1d}$ of $1.16\times0.60$ (1–0.04)$=6.7\times10^{-11}$ cm$^3$ s$^{-1}$. On the other hand the 2006 recommendation (Sander et al., 2006) of $k_{R1d}=6.7\times10^{-11}\exp(20/T)$ gives a rate constant of $7.3\times10^{-11}$ cm$^3$ s$^{-1}$ at 220 K. The IUPAC recommendation (Atkinson et al., 2004) for $k_{R1d}$ is $7.2\times10^{-11}$ cm$^3$ s$^{-1}$, independent of temperature. If we also adopt a branching ratio $k_{R1d}/k_{R1}$=0.60, the present study results in a value for $k_{R1d}$ of $8.3\times10^{-11}$ cm$^3$ s$^{-1}$ at 220 K, which represents significant increases of ca. 15% over the last two values and of 24% over the first.

[1]The rate constant for O($^1$D)+$N_2$ was taken from Blitz et al. (2004), that for O($^1$D)+$N_2O$ was taken from this work, and that for O($^1$D)+$C_2H_2$ was taken from Carl (2005) and assumed to be independent of temperature. The rate constant for $C_2H$+$N_2O$ is taken from recent, unpublished, experiment determinations of this laboratory that shows it to be less than $2\times10^{-14}$ cm$^2$ s$^{-1}$ below 600 K. The rate constant for $C_2H$+$C_2H_2$ was taken to be $1.3\times10^{-10}$ cm$^3$ s$^{-1}$, independent of temperature.

## 4 Conclusions

We have determined the rate coefficient $k_{R1}$ of the reaction O($^1$D)+$N_2O$ over the wide temperature range 227 K–719 K using a new and highly sensitive technique for monitoring O($^1$D), that provides a high $k_{R1}(T)$ measurement precision. We have firmly established that the rate constant has negligible temperature dependence over atmospheric temperature ranges, but shows a pronounced negative temperature dependence for $T > 450$ K. Our $k_{R1}(T)$ data are significantly higher than the current JPL/NASA recommendations. At stratospheric temperatures, at which the title reaction is most important, our rate constant is about 15% above the current recommendation. We have also determined that the minor channel leading to O($^1$D$\rightarrow^3$P) quenching is entirely negligible at all atmospheric temperatures.

*Acknowledgements.* S. V. gratefully acknowledges financial support of the Institute for the Promotion of Innovation through Science and Technology in Flanders (IWT-Vlaanderen) in the form of a Ph.D. grant.

Edited by: A. Hofzumahaus

## References

Amimoto, S. T., Force, A. P., Gulotty Jr., R. G., and Wiesenfeld, J. R.: Collisional deactivation of O($^1$D$_2$) by the atmospheric gases, J. Chem. Phys., 71, 3640–3647, 1979.

Atkinson, R., Baulch, D. L., Cox, R. A., Crowley, J. N., Hampson, R. F., Hynes, R. G., Jenkin, M. E., Rossi, M. J., and Troe, J.: Evaluated kinetic and photochemical data for atmospheric chemistry: Volume I – gas phase reactions of $O_x$, $HO_x$, $NO_x$ and $SO_x$ species, Atmos. Chem. Phys., 4, 1461–1738, 2004, http://www.atmos-chem-phys.net/4/1461/2004/.

Bhardwaj, A. and Haider, S. A.: Chemistry of O$^1$D atoms in the coma: implications for cometary missions, Adv. Space Res., 29, 745–750, 2002.

Blitz, M. A., Dillon, T. J., Heard, D. E., Pilling, M. J., and Trought, I. D.: Laser induced fluorescence studies of the reactions of O($^1$D$_2$) with $N_2$, $O_2$, $N_2O$, $CH_4$, $H_2$, $CO_2$, Ar, Kr and n-$C_4H_{10}$, Phys. Chem. Chem. Phys., 6, 2162–2171, 2004.

Cantrell, C. A., Shetter R. E., and Calvert, J. G.: Branching ratios for the O($^1$D)+$N_2O$ reaction, J. Geophys. Res., 99, 3739–3743, 1994.

Carl, S. A.: A highly sensitive method for time-resolved detection of O($^1$D) applied to precise determination of absolute O($^1$D) reaction rate constants and O($^3$P) yields, Phys. Chem. Chem. Phys., 7, 4051–4053, 2005.

Crutzen, P. J.: Ozone production rates in an oxygen-hydrogen-nitrogen oxide atmosphere, J. Geophys. Res., 76, 7311–7327, 1971.

Crutzen, P. J. and Brühl, C.: Catalysis by $NO_x$ as the Main Cause of the Spring to Fall Stratospheric Ozone Decline in the Northern Hemisphere, J. Phys. Chem. A, 105, 1579–1582, 2001.

Davidson, J. A., Howard, C. J., Schiff, H. I., and Fehsenfeld, F. C.: Measurement of the branching ratios for the reactionof O($^1$D$_2$) with $N_2O$, J. Chem. Phys., 70, 1697–1704, 1979.

Devriendt, K., Van Look, H., Ceursters, B., and Peeters, J.: Kinetics of formation of chemiluminescent CH($A^2\Delta$) by the elementary reactions of $C_2H(X^2\Sigma^+)$ with O($^3$P) and $O_2(X^3\Sigma_g^-)$: A pulse laser photolysis study, Chem. Phys. Lett., 261, 450–456, 1996.

Dillon, T. J., Horowitz, A., and Crowley, J. N.: The atmospheric chemistry of sulphuryl fluoride, $SO_2F_2$, Atmos. Chem. Phys., 8, 1547–1557, 2008, http://www.atmos-chem-phys.net/8/1547/2008/.

Dils, B., Kulkarni, R. M., Peeters, J., and Carl S. A.: Absolute rate coefficients of the reactions of $CF_2(aB_1^3)$ with $C_3H_8$, $C_3H_6$, iso-$C_4H_8$ and$C_3H_4$ between 295 and 550 K, Phys. Chem. Chem. Phys., 6, 2211–2215 , 2004.

Dunlea, E. J. and Ravishankara, A. R.: Kinetic studies of the reactions of O(1D) with several atmospheric molecules, Phys. Chem. Chem. Phys. 6, 2152–2161, 2004.

Elsamra, R. M. I., Vranckx, S., and Carl, S. A.: CH($A^2\Delta$) formation in hydrocarbon combustion: The temperature dependence of the rate constant of the reaction $C_2H+O_2\rightarrow CH(A^2\Delta)+CO_2$, J. Phys. Chem. A. 109, 10 287–10 293, 2005.

Forst, W.: Unimolecular reactions: a concise introduction, Chap. 7, Cambridge University Press, 2003.

Heidner, R. F., Wiesen Jr., F. E., and Husain, D.: Kinetic study of electronically excited oxygen atoms, O($2^1$D$_2$), by time-resolved atomic absorption spectroscopy in the vacuum ultraviolet ($\lambda$=115.2 nm, O($3^1D_2^0 \leftarrow 2^1D_2$)), Chem. Phys. Lett., 16, 530–533, 1972.

Kaspar, T., Tuan, A., Tonkyn, R., Hess, W. P., Rogers, J. W., and Ono, Y. J.: Role of O$^1$D in the oxidation of Si(100), Vac. Sci. Technol., B, 21b, 895–899, 2003, and references therein.

Khamaganov, V. G., Bui, V. X., Carl, S. A., and Peeters, J.: Absolute rate coefficient of the OH + $CH_3C(O)OH$ reaction at $T$=287-802 K. The two faces of pre-reactive H-bonding, J. Phys. Chem A, 110, 12 852–12 859, 2006.

Kharchenko, V. and Dalgarno, A.: Thermalization of fast O($^1$D) atoms in the stratosphere and mesosphere, J. Geophys. Res.-Atoms., 109, D18311, doi:10.1029/2004JD004597, 2004.

Luque, J. and Crosley, D. R.: Electronic transition moment and rotational transition probabilities in CH .1. $A^2\Delta$-$X^2\Pi$ system, J. Chem. Phys., 104, 2146–2155, 1996.

Nair, H., Summers, M. E., Miller, C. E., and Yung, Y. L.: Isotopic fractionation of methane in the martian atmosphere, Icarus, 175, 32–35, 2005.

Nishida, S., Takahashi, K., Matsumi, Y., Taniguchi, N., and Hayashida, S. J.: Formation of O($^3$P) atoms in the photolysis of $N_2O$ at 193 nm and O($^3$P) + $N_2O$ product channel in the reaction of O($^1$D) + $N_2O$, Phys. Chem. A, 108, 2451–2456, 2004.

Sander, S. P., Friedl, R. R., Ravishankara, A. R., Golden, D. M., Kolb, C. E., Kurylo, M. J., Molina, M. J., Moortgat, G. K., Keller-Rudek, H., Finlayson-Pitts, B. J., Wine, P. H., Huie, R. E., and Orkin, V. L.: Chemical Kinetics and Photochemical Data for Use in Atmospheric Studies, Evaluation Number 15, JPL Publication 06-2, National Aeronautics and Space Administration, Jet Propulsion Laboratory, California Institute of Technology, Pasadena, California July 10, 2006.

Selwyn, G., Podolske, J., and Johnston, H. S.: Nitrous-oxide ultraviolet-absorption spectrum at stratospheric temeratures, Geophys. Res. Lett., 4, 427–430, 1977.

Takahashi, K., Takeuchi, Y., and Matsumi,Y.: Rate constants of the O($^1$D) reactions with $N_2$, $O_2$, $N_2O$, and $H_2O$ at 295 K, Chem.

Phys. Lett., 410, 196–200, 2005.

Tamura, M., Berg, P. A., Harrington, J. E., Luque, J., Jeffries, B., Smith, G. P., and Crosley, D. R.: Collisional quenching of CH(A), OH(A), and NO(A) in low pressure hydrocarbon flames, Combust. Flame, 114, 502–514, 1998.

Vakhtin, A. B., Heard, D. E., Smith, I. W. M., and Leone, S. R.: Kinetics of reactions of $C_2H$ radical with acetylene, $O_2$, methylacetylene, and allene in a pulsed Laval nozzle apparatus at T=103 K, Chem. Phys. Lett., 344, 317–324, 2001.

Van Look, H. and Peeters, J.: Rate coefficients of the reactions of $C_2H$ with $O_2$, $C_2H_2$, and $H_2O$ between 295 and 450 K, J. Phys. Chem., 99, 16 284–16 289, 1995.

Wine, P. H. and Ravishankara, A. R.: Kinetics of the $O(^1D)$ interactions with the atmopsheric gases $N_2$, $N_2O$, $H_2O$, $H_2$, $CO_2$, and $O_3$, Chem. Phys. Lett., 77, 103–109, 1981.

Wine, P. H. and Ravishankara, A. R.: $O_3$ Photolysis at 248 nm and $O(^1D_2)$ quenching by $H_2O$, $CH_4$, $H_2$, and $N_2O$ - $O(^3P_J)$ yields, Chem. Phys., 69, 365–373, 1982.